Materials Today Energy 13 (2019) 50–55

Contents lists available at ScienceDirect

Materials Today Energy

journal homepage: www.journals.elsevier.com/materials-today-energy/

Conversion of soybean waste to sub-micron porous-hollow carbon spheres for supercapacitor via a reagent and template-free route

Shanshan Wang [a, b, 1], Wei Sun [c, 1], Dong-Sheng Yang [a, **], Fuqian Yang [b, *]

[a] Department of Chemistry, University of Kentucky, Lexington, KY 40506, United States
[b] Materials Program, Department of Chemical and Materials Engineering, University of Kentucky, Lexington, KY 40506, United States
[c] College of Chemistry, Chemical Engineering and Environmental Engineering, Liaoning Shihua University, Fushun, Liaoning 113001, China

ARTICLE INFO

Article history:
Received 12 March 2019
Received in revised form
29 April 2019
Accepted 30 April 2019

Keywords:
Biomass waste
Hollow-porous structure
Template-free

ABSTRACT

Sub-micron porous-hollow carbon spheres are synthesized from ground soybean waste via a facile and economical hydrothermal carbonization and high-temperature heat-treatment in different media. The sub-micron porous-hollow carbon spheres after the heat treatment with the flow of argon have an average size of 398 ± 10 nm and an average shell thickness of ~40 nm. The carbon in the porous-hollow spheres is amorphous. The electrochemical analyses of the porous-hollow spheres reveal that the porous-hollow carbon spheres heat-treated with the flow of the mixture of N_2 and H_2O steam have good capacitive properties and high specific capacitances, and the porous-hollow carbon spheres heat-treated in an inert medium (N_2 or Ar) possess relatively low capacitances with good rate capability. The results reported in this work likely provide a new and simple route for preparing functional materials with designed structures.

1. Introduction

Carbonaceous materials of submicron sizes offer practical and/or potential applications in energy storage [1], bioengineering [2], pollution control [3], and catalysis [4] among others. These materials can be synthesized via efficient and economical hydrothermal carbonization (HTC), and the HTC-synthesized particles from different precursors under well-controlled hydrothermal conditions exhibit a variety of morphologies, including carbon sphere [5], carbon fiber [6], carbon nanotube [7], and graphene [8,9]. Beside traditional, widely-used commercial chemicals (e.g., glucose [10], xylose [11], starch [12], cellulose [13]), biomass and food wastes are attracting great interests as precursors for hydrothermal syntheses. Peanut shell [14], coconut shell [15], hemp [16], bamboo [17], rice [18], and waste sugar [19] have been used to derive carbonaceous materials via HTC. Tofu and soymilk are two favorite foods for people in East Asia, and are popular worldwide as well. A great amount of ground soybean waste is produced from the production of the soybean-based foods, and it would be desirable to convert this vast waste resource into value-added products.

In this work, we report the synthesis and characterization of porous-hollow carbon spheres from ground soybean waste. Hollow-spherical structure is formed unexpectedly by the HTC process without template. The hollow-spherical structure remains unchanged after the heat treatment at 850 °C in different media. However, the heat treatment leads to the increase of surface area, porosity, and electric conductivity, which vary with the medium used in the heat treatment. The template-free process is much simpler than conventional procedures, involving the synthesis of particles of a core/shell structure with the core as a template, which is then removed by etching [20–26] or annealing [27,28], to form hollow particles. The method reported here may be extended to the syntheses of hollow carbon particles from other biomass wastes.

2. Experimental details

The porous-hollow carbon spheres were synthesized by HTC, followed by annealing at a high temperature. Ground soybean waste of ~40 g was added to deionized (DI) water of ~30 mL with 1 mL 30 *vol*% H_2SO_4, and dispersed ultrasonically. The suspension was poured into a Teflon liner, which was then sealed and placed in a steel autoclave. The HTC processing took place in the Teflon liner

* Corresponding author.
** Corresponding author.
E-mail addresses: dyang0@uky.edu (D.-S. Yang), fyang2@uky.edu (F. Yang).
[1] These authors contributed equally to this work and should be considered as co-first authors.

https://doi.org/10.1016/j.mtener.2019.04.015
2468-6069/

at 200 °C for 20 h in an oven. After cooling down to room temperature in the oven, the HTC-synthesized product was collected by filtration, washed by DI water, dried at 80 °C for 12 h, and then heat-treated in a tube furnace at 850 °C for 2 h with the flow of different gaseous media, including N_2, Ar, and mixture of N_2 and H_2O steam (the flow rate of H_2O steam was 0.1 mm^3/s). The final product was collected without further treatment.

The morphologies of the final products were characterized on a scanning electron microscope (SEM, Hitachi S4300) and a transmission electron microscope (TEM, JEOL 2010F). The surface properties of the final products were measured by a nitrogen adsorption–desorption technique on an automated adsorption analyzer (Micromeritics Surface Characterization, Norcross, GA). The structures were analyzed by X-ray diffraction (XRD) on a Bruker-AXS D8 Advanced X-ray diffractometer equipped with Cu Kα radiation (λ = 1.5406 Å) and by Raman spectroscopy (Thermo Fisher Scientific) equipped with a diode-pumped, frequency-doubled Nd:YVO_4 532 nm laser.

The electrochemical properties of the final products were studied in a three-electrode electrochemical cell. An aqueous suspension with a concentration of 10 mg/mL was prepared from the final products. A droplet of ~3 μL of the as-prepared suspension was dripped onto the surface of a circular carbon-glass current collector, which was dried at 60 °C for 20 min in vacuum to form a thin film with a loading mass of ~0.03 mg. The counter and reference electrodes were a platinum plate and a set of Ag/AgCl electrode, respectively. The electrolyte was a 1.00 mol/L Na_2SO_4 solution. Cyclic voltammetry (CV) and electrochemical impedance spectroscopy (EIS) were performed on a Princeton electrochemical workstation (PARSTAT MC).

3. Results and discussion

Fig. 1 shows SEM (a, b) and TEM (c–f) images of the HTC-synthesized carbon particles before and after the heat treatment with the flow of argon. The embedded plots in Fig. 1a and b depict the size distribution of the carbon spheres. The HTC-synthesized carbon particles are spherical (Fig. 1a) and hollow (Fig. 1c). The heat treatment reduces the sizes of the carbon spheres (Fig. 1b) and causes slight changes in the topology, while it does not change the hollow structure of the carbon particles (Fig. 1d). The average size of the carbon spheres is 520 ± 13 nm prior to the heat treatment and

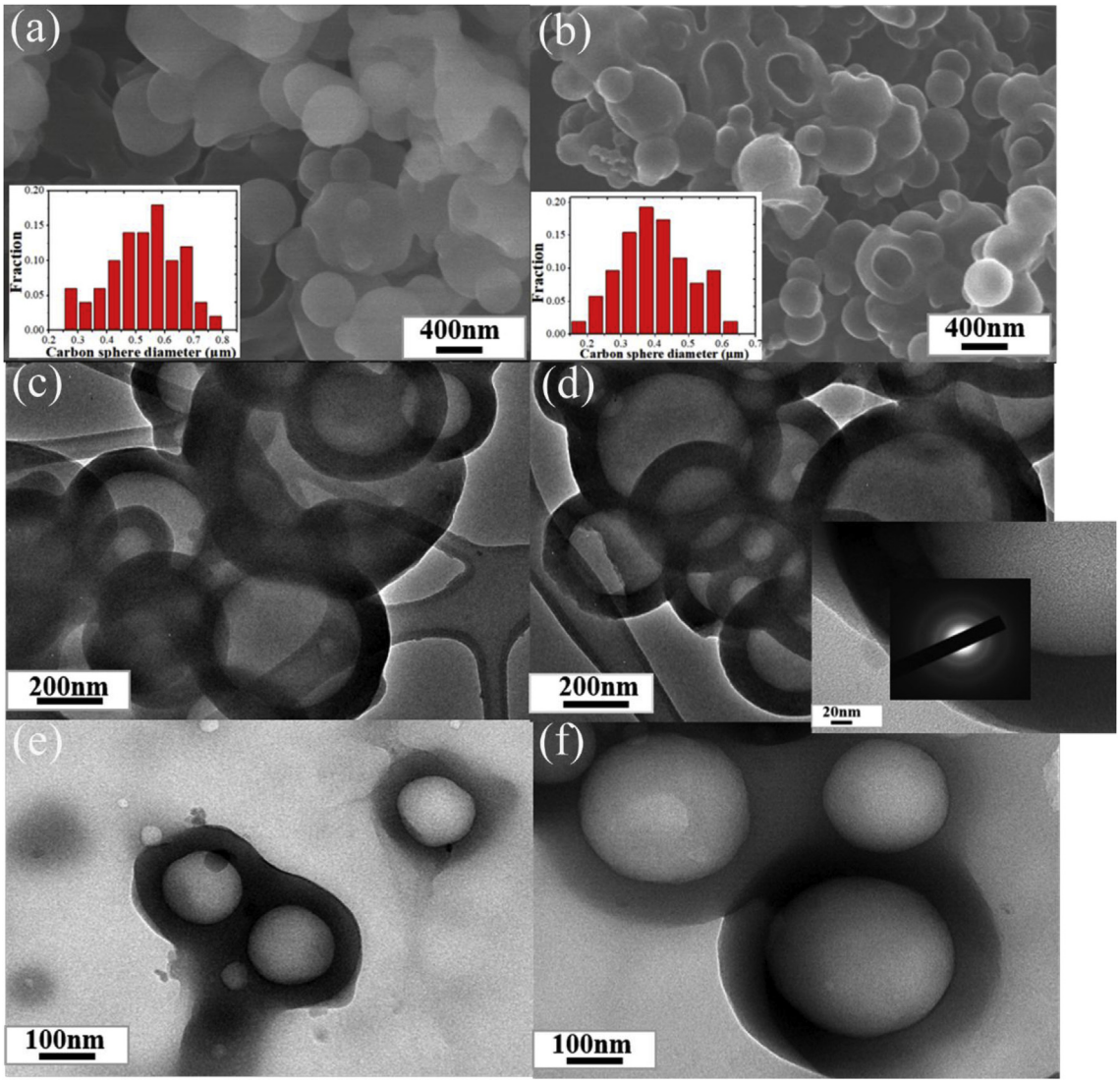

Fig. 1. SEM images of the carbon spheres produced by HTC process: (a) before and (b) after heat treatment with the flow of argon; TEM images of the carbon spheres: (c) before and (d–f) after heat treatment with the flow of argon.

398 ± 10 nm afterwards. Carbon spheres with single hole (Fig. 1e) and twin holes (Fig. 1f) are observed. The average shell thickness is ~40 nm. The inset in Fig. 1d is the selected area electron diffraction of the shell, revealing that the shell of the hollow carbon spheres is amorphous. Note that the hollow carbon spheres heat-treated in other gaseous environments have similar structures and average particle size to the carbon spheres heat-treated with the flow of argon.

Fig. 2a shows the XRD patterns of the hollow carbon spheres before and after the heat treatment in different gaseous environments, respectively. There is a broad peak at $2\theta = \sim 23^\circ$ for all the prepared hollow carbon spheres, confirming that the hollow carbon spheres are amorphous. The small peak at $2\theta = \sim 43^\circ$ for the heat-treated hollow carbon spheres, corresponding to the (100) plane of graphitic carbon, implies that the heat treatment increases the crystallinity of the amorphous carbon [29,30].

Fig. 2b depicts the Raman spectra of the HTC products and heat-treated hollow carbon spheres. There are two Raman peaks present for all the materials; one represents the D band caused by the presence of sp [3] carbons, and the other is the G band from the sp^2-carbon in-plane vibration of graphite [31]. The heat treatment causes the shift of both D and G bands. The wavenumber of the D band shifts from 1371 cm^{-1} for the HTC products to 1344 cm^{-1}, 1348 cm^{-1}, and 1348 cm^{-1} for the heat-treated hollow carbon spheres with the flow of Ar, N_2 and N_2/H_2O steam, respectively, and the wavenumber of the G band is around 1582 cm^{-1} for all the carbon spheres.

It is known that the integrated intensity ratio of I(D)/I(G) can represent the degree of structural order and the density of edge planes in sp^2-bonded carbon particles [32]. Using the Gaussian deconvolution, the integrated intensity ratios of I(D)/I(G) are calculated to be 3.04 for the HTC sample, 1.98 for the carbon spheres heat-treated with the mixture of N_2 and H_2O steam, 2.12 for the carbon spheres heat-treated with N_2, and 2.09 for the carbon spheres heat-treated with Ar, respectively. The band shift and ratio change due to the heat treatment suggest that the heat treatment increases the structural order and average size of the graphitic domains of the hollow carbon spheres.

Fig. 2c depicts the nitrogen adsorption–desorption curves of the hollow carbon spheres heat-treated with the flow of three different gases. The isotherm curves of all the three samples exhibit a Type I profile, indicating the presence of microporous structures and narrow slit-like pores in the porous hollow spheres [33]. From the nitrogen adsorption–desorption isotherm, the size distribution of the pores is calculated and shown in Fig. 2d. The pores in the hollow carbon spheres activated with the flow of the mixture of N_2 and H_2O steam have a broad distribution of the pore sizes in a range of 0.5–4 nm. The pores in the hollow carbon spheres activated with the flow of N_2 or Ar have relatively narrow distribution of the pore sizes, and the pores in the carbon spheres activated with the flow of N_2 are generally larger than those in the hollow carbon spheres activated with the flow of Ar. These results reveal the formation of micropores in the hollow carbon spheres after the heat treatment and the dependence of the porous structures on the gas used in physical activation at high temperatures.

Table 1 summarizes the surface properties of the hollow carbon spheres. It is evident that the physical activation at 850 °C for 2 h leads to the formation of porous structures and the increase of surface area of the hollow carbon spheres. The surface area and porosity of the hollow carbon spheres activated with the flow of the mixture of N_2 and H_2O steam are significantly larger than the hollow carbon spheres activated with the flow of N_2 or Ar, and the largest pores are present in the hollow carbon spheres activated with the flow of the mixture of N_2 and H_2O steam. H_2O steam is an effective agent for the physical activation of carbon microspheres.

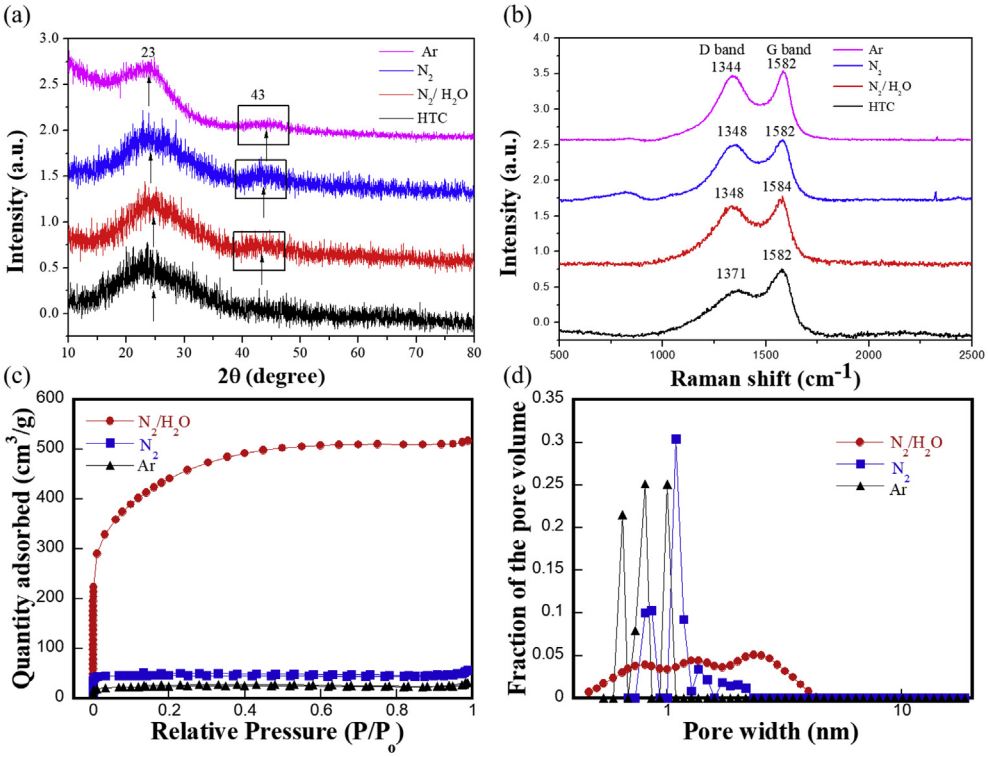

Fig. 2. Characterizations of the hollow carbon spheres: (a) XRD patterns, (b) Raman spectra with D and G bands fitted with Gaussian lines, (c) nitrogen adsorption–desorption isotherm, and (d) distribution of pore sizes calculated from the adsorption–desorption isotherm via density functional theory for the heat-treated hollow carbon spheres.

Table 1
Surface properties of hollow carbon microspheres.

Material		BET surface area (m^2/g)	Pore volume (cm^3/g)	Pore size distribution (%)			
	Gas			0–1 nm	1–2 nm	2–50 nm	>50 nm
Activated carbon spheres	$H_2O + N_2$	1077.67	0.68	30.9	36.3	32.8	0
	N_2	161.95	0.07	54.6	25	0	20.4
	Ar	85.85	0.04	50.7	20.6	0	29.7
HTC product	N/A	1.91	0.01	N/A	N/A	N/A	N/A

The mechanism of the H_2O-steam activation can be expressed as follows [34],

$$C^* + H_2O \rightarrow C{\cdot}H_2O \rightarrow \begin{cases} C \cdot O \rightarrow CO \\ C^* H_2 \rightarrow C \cdot H_2 \end{cases}$$

In general, the reactions between the carbon matrix and the H_2O steam lead to the formation of new micropores and/or the growth of pre-existing ultra-micropores [35]. According to Table 1, N_2 seems to be more effective than Ar in activating carbon microspheres physically. Note that the pore volume for the large pores (>50 nm) may be attributed to the separation between carbon spheres.

A three-electrode electrochemical cell was constructed to characterize the electrochemical behavior of the heat-treated porous-hollow carbon microspheres. Fig. 3a shows CV curves of the three different heat-treated carbon microspheres at a scan rate of 0.05 V/s in a working voltage window of −0.2 V to 0.8 V (vs the Ag/AgCl reference electrode). The CV curves exhibit quasi-rectangular shape for all the carbon microspheres activated physically with the flow of different gases, indicating good capacitive behavior.

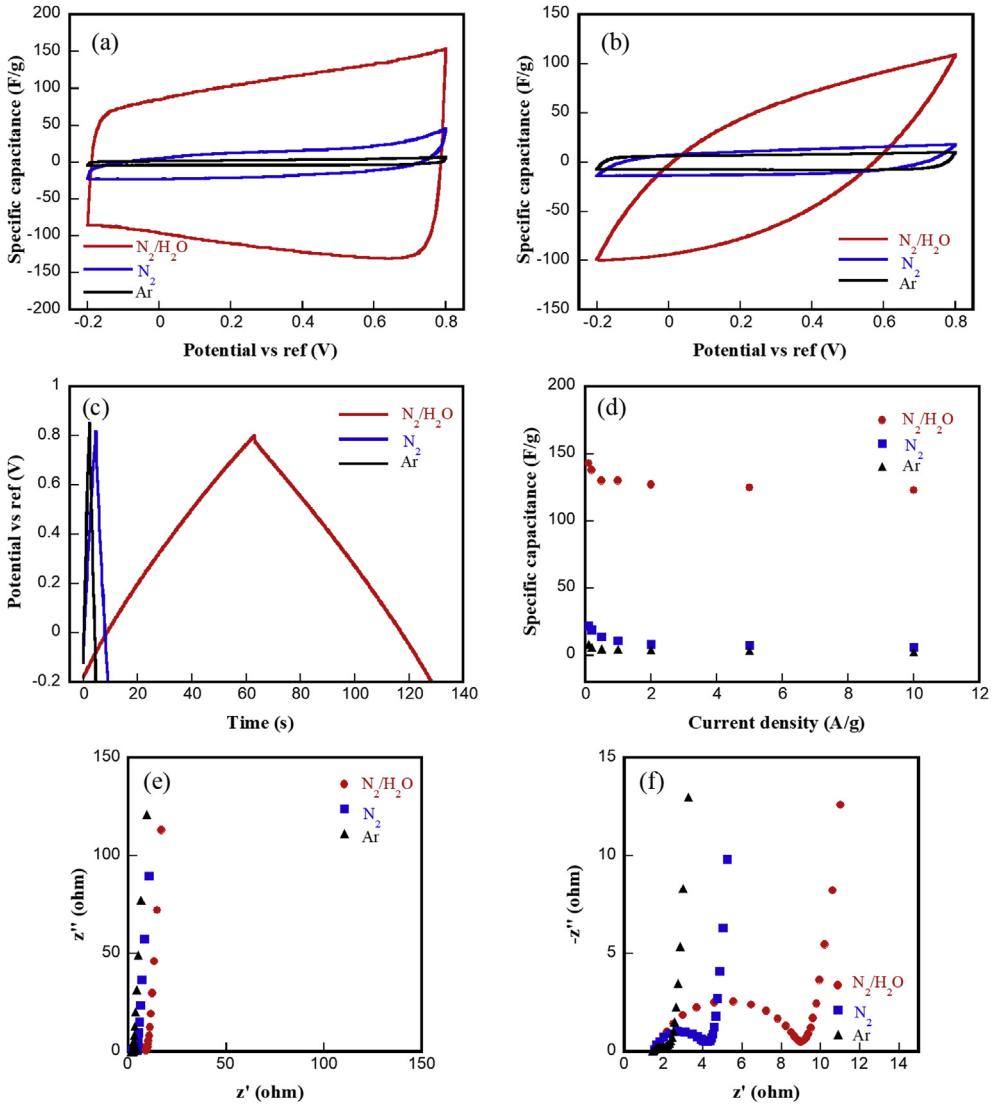

Fig. 3. Electrochemical characteristics of porous-hollow carbon spheres: (a) CV curves at a scan rate of 0.05 V/s, (b) CV curves at a scan rate of 1.0 V/s, (c) Galvanostatic charging–discharging (GCD) curves measured at a current density of 1 A/g, (d) variation of specific capacitance as a function of current density, (e) Nyquist plots at an open circuit voltage of −0.2 V, and (f) an enlarged view of the Nyquist plots for the semi-circles.

Table 2
Electrochemical properties of porous-carbon microspheres activated with the flow of three different gasses.

Material	Gas	$C_{0.1}$ (F/g)	C_{10} (F/g)	$C_{10}/C_{0.1}$	R_s (Ohm)	R_f (Ohm)
Activated carbon spheres	$H_2O + N_2$	143	123	0.86	1.79	9.02
	N_2	22	6	0.27	1.54	4.15
	Ar	8.4	2.8	0.33	1.44	2.04

Note: $C_{0.1}$ is the specific capacitance measured at a current density of 0.1 A/g, and C_{10} is the specific capacitance measured at a current density of 10 A/g at the first cycle.

It is known that the area enclosed by the CV curve represents the storage of charges in the working electrode. From Fig. 3a and b, we can conclude that the porous carbon microspheres activated with the flow of the mixture of N_2 and H_2O steam possess the largest specific capacitance in accord with the presence of the significant amount of surface areas.

Fig. 3b shows the CV curves of the three different heat-treated carbon microspheres at a relatively high scan rate of 1 V/s. The CV curves for the carbon microspheres activated with the flow of N_2 or Ar maintain quasi-rectangular shape, suggesting fast migration/diffusion of ions into porous carbon microspheres even under a high scan rate. Such behavior is in accord with the increase of the driving force with the increase of voltage. However, a spindled CV curve is observed for the carbon microspheres activated with the flow of the mixture of N_2 and H_2O steam, indicating less favorable capacitive behavior under a high scan rate than under a small scan rate.

Fig. 3c shows the galvanostatic charging–discharging (GCD) curves measured at a current density of 1 A/g for the three different heat-treated carbon microspheres. Both the charging and discharging curves are relatively linear functions of the charging/discharging time, and exhibit good mirror-symmetry, confirming good capacitive behavior of the heat-treated carbon microspheres. There is no significant voltage drop (IR drop) for all the heat-treated carbon microspheres at this current density, indicating that the heat-treated carbon microspheres have good conductivity.

The specific capacitance is calculated from the discharging portion of the GCD curve as

$$C = \frac{2I}{m}\left(\frac{dV}{dt}\right)^{-1} \quad (1)$$

where I is electric current intensity, m is the mass of activated carbon microspheres on the working electrode, and dV/dt is the slope of the discharge curve after the voltage drop. Fig. 3d shows the variation of the specific capacitance with the current density for the carbon spheres activated with the flow of different gases. For the same current density, the carbon microspheres activated with the flow of the mixture of N_2 and H_2O steam possess a significantly higher specific capacitance than the carbon spheres activated with the flow of N_2 and Ar. Such a trend revels the important role of the surface area and porous structures in controlling the storage of charges in carbon microspheres. For all the electrochemical systems, the specific capacitance decreases with the increase of the current density. The carbon microspheres activated with the flow of the mixture of N_2 and H_2O steam have good retention in capacitance, which is 143 F/g at 0.1 A/g and 123 F/g at 10 A/g measured at the first circle.

Table 2 summarizes the electrochemical properties of the carbon microspheres activated with the flow of three different gasses. Comparing with the steam-activated biomass-derived carbons reported in literature, we note that the soybean-derived hollow carbon microspheres exhibit higher or comparative specific capacitance. For instance, the activated carbons derived from Oil-Palm-Kernel Shell possess a specific capacitance of 123 F/g at a current density of 0.5 A/g [36]; the Corncob-residue-derived activated carbons have a specific capacitance of 120 F/g at a current density of 1 A/g [37]; and the specific capacitance measured at a scan rate of 10 mV/s is 105 F/g for the activated carbons derived from Fir wood [38].

EIS analyses of the three different activated hollow carbon microspheres in the three-electrode electrochemical cell were performed at an open circuit voltage of −0.2 V and in the frequency range of 0.01 Hz–1 MHz. Fig. 3e shows the Nyquist plot of the three activated hollow carbon microspheres. It is evident that there is a sharp increase of $-z''$ in the region of low frequencies for all the activated hollow carbon microspheres, suggesting that all the three activated hollow carbon microspheres possess good capacitive behavior in accord with the results shown in Fig. 3a.

Fig. 3f shows the enlarged view of the Nyquist plot in the range of high frequencies. All the three activated hollow carbon microspheres have smaller resistance than the carbonaceous electrode materials reported by Sun et al. [16]. The semi-cycles presented in the Nyquist plots in the range of high frequencies suggest that the working electrodes made from the activated hollow carbon microspheres can be approximated as an electric system consisting a resistance and a capacitance in parallel connection.

From Fig. 3f, we can calculate the system resistance, R_s, including the intrinsic resistances of electrolyte and the contact resistance between electrode and current collector, and the resistance, R_f, to the migration of electrolyte ions in the pores of electrode materials from the intercepts of the Nyquist plots with the z' axis. Table 2 lists the values of R_s and R_f. There is no significant difference of R_ss for all the three different carbon microspheres, suggesting the consistence of the electrochemical cell structures. The carbon microspheres activated with the flow of the mixture of N_2 and H_2O steam have the largest R_f, and the carbon microspheres activated with the flow of Ar have the smallest R_f. Such a trend is likely associated with the fraction of the pores with sizes larger

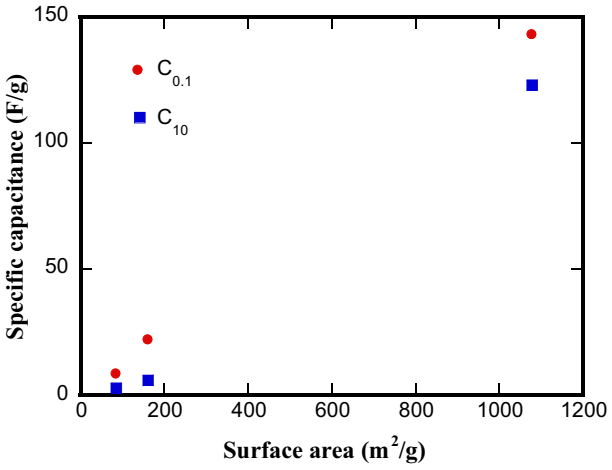

Fig. 4. Variation of specific capacitance with BET surface area.

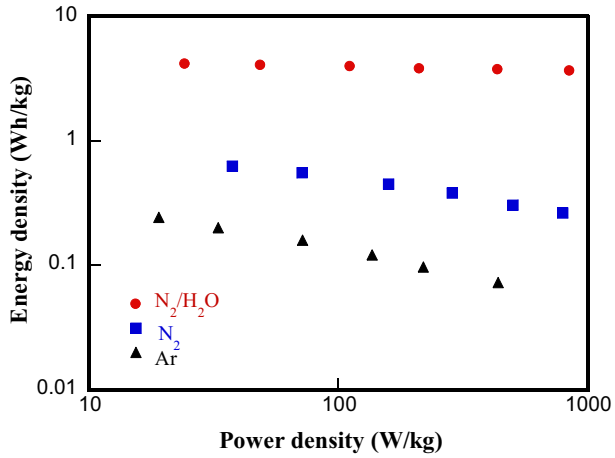

Fig. 5. Ragone plot of the hollow carbon spheres.

than 50 nm. According to Table 1, the carbon microspheres activated with the flow of Ar have 29.7% of pores with sizes larger than 50 nm, and the carbon microspheres activated with the flow of the mixture of N_2 and H_2O steam have no pores with sizes larger than 50 nm. The larger the pore size, the smaller is R_f.

Using the data in Tables 1 and 2, the variation of the specific capacitance with the BET surface area is shown in Fig. 4. The specific capacitances measured at the current densities of 0.1 A/g and 10 A/g increase with the increase of the surface area. Increasing the porosity and surface area can significantly increase the storage of charges in porous-carbon spheres per unit mass.

The energy density of E and power density of P were calculated for a symmetric cell according to the following equations,

$$E = \frac{1}{2} \times C_s V^2 \text{ and } P = \frac{E}{t} \quad (2)$$

where C_s is the specific capacitance of the symmetric cell, V is the voltage excluding the IR drop, and t is time after the IR drop. Fig. 5 shows the Ragone plot of the hollow carbon spheres activated with different conditions. The hollow carbon spheres activated with the flow of the mixture of N_2 and H_2O steam exhibit significantly higher energy density and power density than the carbon spheres activated with the flow of pure N_2 and Ar. Also, the retention of the energy density of the carbon spheres activated with the flow of the mixture of N_2 and H_2O steam is also superior to the carbon spheres activated in pure inert gas flows. Such results suggest that the H_2O-steam-activated hollow carbon spheres with high surface area and microporous structures possess good electrochemical properties.

4. Conclusions

In summary, porous-hollow carbon spheres of submicron sizes have been synthesized from soybean waste via a simple route without any templates. The simple route consists of hydrothermal carbonization and heat treatment at 850 °C with the flow of different gases. The hydrothermal carbonization leads to the formation of hollow carbon spheres of submicron sizes; the heat treatment reduces the sizes of the carbon spheres, improves structural ordering, and forms micropores in the hollow carbon spheres.

The porous-hollow carbon spheres exhibit good capacitive properties, which depend on the gas used in the physical activation. The carbon spheres heat-treated with the flow of the mixture of N_2 and H_2O have the largest specific capacitance of 143 A/g and good capacitance retention of 0.86. The carbon spheres heat-treated with the flow of inert gases (N_2 and Ar) have relatively low capacitances, and exhibit good capacitive behavior at high scan rates. Such structures likely have potential applications in the supercapacitors with high charging rates.

The raw data required to reproduce these findings are available to download from http://web.engr.uky.edu/~fyang0/.

Acknowledgment

This work is supported by the NSF through the grant CMMI-1634540 (FQY) monitored by Dr. Khershed Cooper, the grant CHE-1800316 (DSY) of Division of Chemistry, and the National Natural Science Foundation of China (No. 21805123) (WS).

Appendix A. Supplementary data

Supplementary data to this article can be found online at https://doi.org/10.1016/j.mtener.2019.04.015.

References

[1] G. Che, et al., Nature 393 (6683) (1998) 346.
[2] A. Bianco, et al., Chem. Commun. (5) (2005) 571.
[3] D.R. Simpson, Water Res. 42 (2008) 2839.
[4] R. Demir-Cakan, et al., Catal. Today 150 (2010) 115.
[5] Y. Fan, et al., J. Power Sources 268 (2014) 584.
[6] H.-S. Qian, et al., Chem. Mater. 18 (2006) 2102.
[7] K. Dai, et al., Appl. Surf. Sci. 270 (2013) 238.
[8] X. a. Chen, et al., J. Power Sources 243 (2013) 555.
[9] H. Wang, et al., ACS Nano 7 (2013) 5131.
[10] R. Demir-Cakan, et al., Chem. Mater. 21 (2009) 484.
[11] M.-M. Titirici, et al., Green Chem. 10 (2008) 1204.
[12] S.-H. Yu, et al., Adv. Mater. 16 (2004) 1636.
[13] M. Sevilla, A.B. Fuertes, Carbon 47 (2009) 2281.
[14] M.D. Huff, et al., J. Environ. Manag. 146 (2014) 303.
[15] A. Jain, et al., Sci. Rep. 3 (2013) 3002.
[16] W. Sun, et al., Carbon 103 (2016) 181.
[17] D. Schneider, et al., Int. J. Energy Environ. 2 (2011) 647.
[18] X. Cui, et al., Small 2 (2006) 756.
[19] Z.-Q. Hao, et al., J. Power Sources 361 (2017) 249.
[20] X. Li, et al., Electrochim. Acta 270 (2018) 1.
[21] R. Liu, et al., Angew. Chem. Int. Ed. 50 (2011) 6799.
[22] T. Yang, et al., J. Mater. Chem. 2 (2014) 18139.
[23] D.-S. Bin, et al., J. Am. Chem. Soc. 139 (2017) 13492.
[24] S. Feng, et al., Chem. Commun. 50 (2014) 329.
[25] G. Wang, et al., Mater. Lett. 197 (2017) 71.
[26] Y. Wang, et al., J. Electrochem. Soc. 164 (2017) A1918.
[27] B. Réti, et al., Catal. Today 284 (2017) 160.
[28] J. Zang, et al., Electrochim. Acta 260 (2017) 783.
[29] R. Andrews, et al., Carbon 39 (2001) 1681.
[30] H. Zhu, et al., Carbon 99 (2016) 174.
[31] K.N. Kudin, et al., Nano Lett. 8 (2008) 36.
[32] G. Chen, et al., J. Appl. Phys. 95 (2004) 1455.
[33] K.S. Sing, Pure Appl. Chem. 57 (1985) 603.
[34] M.G. Plaza, et al., Appl. Energy 114 (2014) 551.
[35] Y.-J. Heo, S.-J. Park, Energy 91 (2015) 142.
[36] I.I. Misnon, et al., Electrochim. Acta 174 (2015) 78.
[37] W.-H. Qu, et al., Bioresour. Technol. 189 (2015) 285.
[38] F.-C. Wu, et al., J. Power Sources 144 (2005) 302.